J. Water Environ. Nanotechnol., 7(3): 267-287 Summer 2022

ORIGINAL RESEARCH PAPER

Optimization and Numerical investigation of organic dye degradation using Response Surface by green synthesized ZrO_2 nanoparticles and its antibacterial activity

A. Ananda[1], T. Ramakrishnappa[2], T.N. Ravishankar[3], S. Archana[4], B.M. Shilpa[5], L.S. Reddy Yadav[2], B.K. Jayanna[6*]

[1] Dayananda Sagar Academy of Technology and Management, Kanakapura Road, Udayapura, Karnataka, India
[2] BMS Institute of Technology and Management, Yelahanka, Bengaluru, Karnataka, India
[3] Centre for Nanoscience and Nanotechnology, Department of Chemistry, Global Academy of Technology, Bangalore, Karnataka, India
[4] Department of Basic Sciences, Faculty of Engineering, Jain University, Bangalore, Karnataka, India
[5] Dayananda Sagar University, School of Basic and Applied Sciences, Kumaraswamy Layout, Bengaluru, Karnataka, India
[6] Department of Chemistry, BNM Institute of Technology, Bangalore

Received: 2022-05-08 Accepted: 2022-06-29 Published: 2022-07-01

ABSTRACT

In this work, the tetragonal Zirconium oxide (ZrO_2) nanoparticles (NPs) were successfully synthesized by solution combustion method using Zirconium (IV) oxynitrate hydrate as the metal precursor and an oxidizer, Basella alba raw extract at 6000C. In this study, natural fuel is used to avoid harmful chemical fuels that may pollute the environment during combustion. The impact of the fuel-to-oxidant molar ratio on the surface morphological features of nanocrystalline zirconia particles has been documented. We investigated the Physico-chemical properties of the ZrO_2 NPs via thorough characterizations like XRD, EDS, SEM, TEM, FTIR, UV-Vis, and BET. ZrO_2 NPs exhibit perfect photocatalytic degradation activity towards Evans blue, a toxic dye. The influence of contact time, initial dye concentration, and pH were among the independent variables used in the study. The Response Surface Model (RSM) was used to optimize and describe the interdependencies of the different variables. The method was evaluated using the Box-Behnken design (BBD). A second-order polynomial model was used to properly understand the experimental results, and the effectiveness of the chosen model was verified by the strong agreement in determination coefficient values. ZrO_2 NPs also exhibit good antibacterial activity on Gram-negative *Klebsiella pneumoniae* and Gram-positive bacteria, *Bacillus subtilis*.

Keywords: *solution combustion, natural fuel, photocatalytic activity, RSM, Evans Blue dye, antibacterial activity.*

How to cite this article
Ananda A., Ramakrishnappa T., Ravishankar T.N., Archana S., Shilpa B.M., Reddy Yadav L.S., Jayanna B.K. Optimization and Numerical investigation of organic dye degradation using Response Surface by green synthesized ZrO_2 nanoparticles and its antibacterial activity. J. Water Environ. Nanotechnol., 2022; 7(3): 267-287.
DOI: 10.22090/jwent.2022.03.004

INTRODUCTION

Amongst various metal oxide nanomaterials, ZrO_2 nanoparticles (ZrNP) have created interest among the current researchers because of their well-known physicochemical properties like hardness, wear resistance, and thermal shock resistance due to toughness and high strength. These unique properties of ZrNPs have resulted in the use of ZrO_2-based components in many industrial applications, including refractory ceramics, oxygen sensors, photocatalysts,

* Corresponding Author Email: *bkjayanna83@gmail.com*

antibacterial, fuel cells, jewelry field, wire-drawing, automobile engine parts, and cutting tools [1,2]. Recently few studies proved the versatility of ZRNPs. Parnian et.al showed that by loading different concentrations of Zirconia on the Nafion nanocomposite membrane, the physicochemical and electrochemical properties of the proton exchange membrane fuel cell can be enhanced [3]. Debnath et. al used zirconia nanocomposite as an alternative adsorbent for the bioremediation of tetracycline present in wastewater, up to 526.32 mg/g [3]. Anticancer and antibacterial activity was studied by Tabassum et. al. ZrO_2 nanoparticles display a concentration-dependent effect on the MDA-MB-231 cell line and antibacterial activity on gram-negative bacteria (*K. pneumoniae*) [4]. Shao et. al., showed that by doping Zr nanoparticles to TiO_2, the photocatalytic activity on Methylene Blue can be enhanced up to 2.2 times than that of the pure TiO_2 [5]. The use of ZrNPs as photocatalysts for the degradation of dyes and antibacterial activities is of our research interest. According to a WHO report, dyes are toxic and one of the major pollutants that cause environmental (water) pollution. The primary sources of dyes are textiles, paper, plastic, and related sectors [3,4]. Recent studies reported that organic dyes in wastewater are causing severe problems to the environment and public health [5,6]. Out of different organic dyes, Evans blue is one of the most widely used dyes in industries. Evans blue, an azo dye reported as toxic and has a highly stable complex structure, contributes majorly to water pollution [7]. So, there is a necessity to convert stable, toxic dye into its non-toxic form using efficient and economical methods [8,9]. Various ways are available for the total elimination of hazardous dyes found in water like physical methods, chemical/photocatalytic degradation of dyes, electrochemical process, and biological methods [10]. Among these methods, the photocatalytic degradation of dyes using UV or UV-Visible light sources is considered the most well-known technique because the reactions are conducted in cost-effective conditions and have simple procedures [11]. Various methods to prepare ZrNPs include such as microwave irradiation[12], sol-gel [13], laser ablation [14], aqueous precipitation method [15],

sonochemical method [16], spray pyrolysis [17], solvothermal [18], and ionic liquid microemulsion [19].These synthetic techniques necessitate high temperatures and pressures, extended reaction times, expensive and hazardous chemical precursors, and the use of specialized instruments for experimental work, all of which have a detrimental environmental impact. This emphasizes the urgent need to develop a simple, clean, non-toxic, and ecologically friendly procedure using green synthesis and other biological approaches to replace chemical preparation methodologies. Solution combustion synthesis has been considered more effective than the other methods as it is deemed to be simple, instantaneous, single-step, and energy-saving [20]. Recently, the solution combustion process is used to manufacture NPs using biobased fuels. Basella alba is one such plant extract that attracts research attention in solution combustion synthesis. A good source of vitamin A, vitamin C, folic acid, iron, magnesium, calcium, and many vital antioxidants are provided by Basella alba. The plant consists of vital amino acids, including arginine, tryptophan, lysine, threonine, leucine, and isoleucine, and specific vitamins, minerals, and a small proportion of soluble oxalates. [21] Though it is used as the fuel for the synthesis of ZrNPs, regulation of synthesis factors such as pH, temperature, substrate concentration, reaction rate, and dosage of extracts has not been studied. Our study concentrates on these aspects to synthesize ZrNPs.

The ZrNP also reported being superior antimicrobial agents to conventional organic antibacterial agents because metal oxide nanoparticles are considered safe, durable, and heat resistant [12]. We have used two bacterial strains for antimicrobial evaluation: Gram-negative *Klebsiella pneumoniae* and Gram-positive bacteria *Bacillus subtilis*.

The current work includes the production of ZrNPs with Zirconium (IV) oxynitrate hydrate as a metal precursor and Basella alba raw extract as an oxidant, at 600 °C. Natural fuel is used here, and it is not toxic, inexpensive, and abundant in carbon, nitrogen, hydrogen, and Oxygen, which are emitted during the combustion process as their respective oxides. This research article emphasizes the characterization of synthesized ZrNPs and their use in photocatalytic degradation of Evans blue dye. For optimization of the degradation process, the one-factor-at-a-time method has typically been used. However, this strategy is time-consuming and costly. It also doesn't look at how variables relate to each other. Hence, the degradation process was optimized in the second phase using response

surface methodology (RSM), an effective and commonly used experimental design methodology, to ensure complete degradation. For optimizing a series of experiments and studying the impact of the existence of multiple control parameters using the series of runs built on the Box-Behnken model are adopted [13,14]. The regeneration and reuse of the synthesized nanohybrid were investigated under optimal conditions and antimicrobial activity against two bacterial strains, Gram-negative *Klebsiella pneumoniae,* and Gram-positive bacteria *Bacillus subtilis*.

EXPERIMENT AND METHODS

Chemicals and reagents

Zirconium (IV) oxynitrate hydrate ($ZrO(NO_3)_2.xH_2O$, and Evans Blue (AR grade) were purchased from Sigma Aldrich. Sodium hydroxide (NaOH), Sulfuric acid (H_2SO_4) was bought from Merck, India. The analytical quality reagents were used with no purifying. All through the research, double distilled water was used.

Preparation of Basella Alba raw extract as Natural fuel for the solution combustion method

500 g of fresh leaves of Basella Alba plant leaf taken from Shivamogga, Karnataka, India. Tiny bits were finely chopped, and 250 mL of double-distilled water was added to it. And these bits are well processed at room temperature to extract form to prepare the extract. Afterward, the extract was filtered by using Whatman filter paper. The resulting extract can be used to synthesize of ZrNPs as fuel for the solution combustion process. Image of Basella Alba leaves and their extract form as given in Scheme.1 (a) and Scheme.1 (b), respectively.

Preparation of ZrNPs using Basella Alba raw extract as natural fuel through solution combustion method

The ZrNPs were synthesized by weighing 2.3123 g of Zirconium (IV) oxynitrate hydrate, and it is transferred into a silica crucible and then dissolved using 15 mL of distilled water. To the above salt solution, 5.0 mL of Basella Alba raw extract is added as a natural fuel and stirred for 5 minutes at 300 rpm to obtain a homogeneous solution at room temperature to form a redox solution. The redox mixture was maintained in a preheated muffle furnace at 400 °C. In just 5 minutes, the reaction gets completed, and a highly foamy and porous material was collected by generating fewer gases. The obtained compound was calcined at 600 °C for 2 hours. To understand the impact of Basella Alba raw extract concentration on the ZrNPs, we have varied four different volumes of fuel (5.0 mL-20 mL). The final products are given the names, ZO1, ZO2, ZO3, and ZO4 for 5.0 mL, 10 mL, 15 mL, and 20 mL volumes of fuel, respectively [15–17] The flow chart for the synthesis of ZrNPs can be depicted in **Scheme.2.**

Characterization

Powder X-ray diffraction (XRD) data were recorded on Philips X'pert PRO X-ray diffractometer with graphite monochromatized Cu-K_α (1.5418 Å) radiation operated at 40 kV and 30 mA. The absorption spectrum of the samples was analyzed using the Perkin Elmer Lambda-750 UV-Vis spectrometer to diffuse NPs in water. The surface morphology was investigated by using Hitachi 3000 scanning electron microscopy (SEM). The sample nanostructure was examined by transmission electron microscopy (TEM) conducted with JEOL JEM 1200 Ex, operating at 100 kV. TEM specimens were produced by placing the 2-propanol metal oxide nanoparticle diffusion on a holey carbon grid and vacuum drying the grids for 24 hours. For BET surface area, i.e., N_2 adsorption-desorption measurements, the extracts were assessed with the help of Tristar II, Micromeritics. All pH measurements were carried out using a digital pH meter MK VI of Systronics makes. The Fourier transform infrared spectra (FTIR) of the samples were collected using a Bruker Alpha-P spectrometer.

Preparation of EB dye solution

Appropriate quantities of EB dye were dissolved in double distilled water to obtain different ppm dye concentration solutions. The solution was kept for 24 hours for the complete dissolution of the dye. The dye solution was stirred adequately before starting the experimental procedure.

Experimental procedure for degradation of EB dye

Photocatalytic reactions were carried out in a setup reactor with the help of 6UV-A lamps (Philips, India). The maximum emission intensity was carried out at 365 nm. The solution and the source were separated by 16 cm. The tests were conducted at room temperature. To calibrate the radiation intensity at the sample site in the testing chamber, radiation detectors or radiometers are utilized. These radiometers constitute amplifying

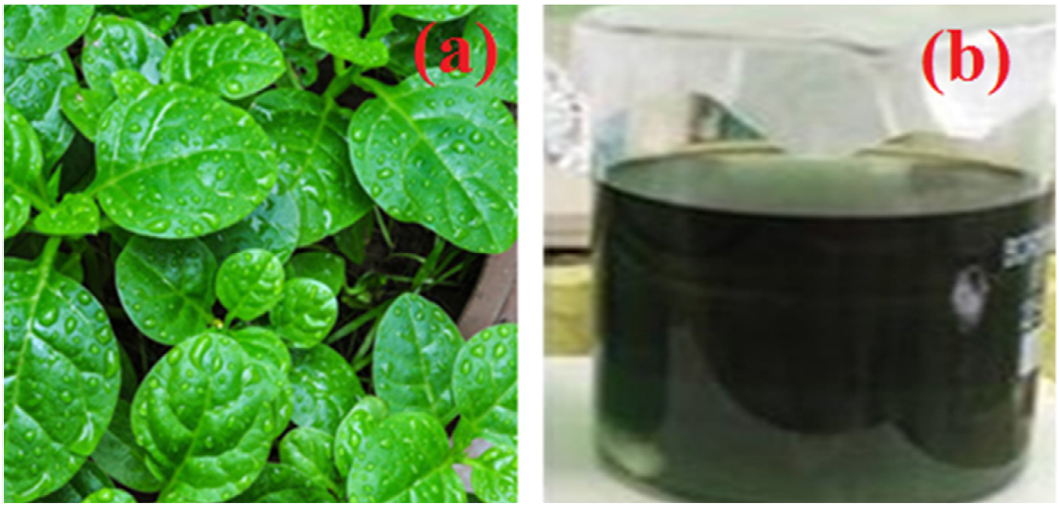

Scheme .1. (a) & (b). Image of Basella Alba leaves, and its extract form and Image of Basella Alba extract form.

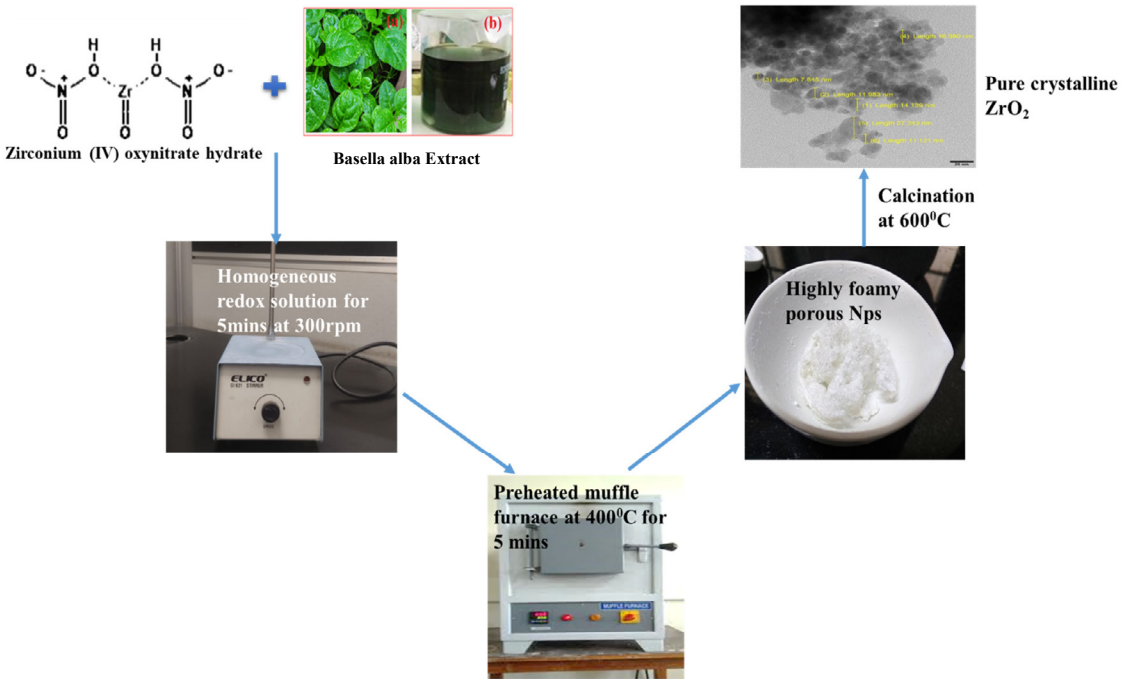

Scheme.2. The scheme for the preparation of ZrNP (ZO3)

circuits, detectors, and displays. Detectors generally consist of diffusers, filters, and silicon photodiodes. Degradation experiments were performed under sunlight in July and August in Karnataka, India, between 9 am and 4 pm. NaOH/ H_2SO_4 is used to adjust the pH of the solution. The efficiency of degradation was determined using the equation:

$$\ln\left(\frac{C_0}{C}\right) = kt \quad (1)$$

$$\text{Degradation efficiency}(\%) = \left(\frac{C_0 - C}{C_0}\right) \times 100 \quad (2)$$

C_0 represents the dye's initial concentration, and after degradation, C is the dye's solution concentration. [15].

Experimental Design Statistical Analysis

RSM-based Box–Behnken design (BBD)

Table 1. Variables and their corresponding levels used in the optimization for adsorption of EB on ZrO_2

Variables	Real values of coded levels		
	-1	0	1
Time (A) in minutes	5	32.5	60
pH (B)	2	7	12
Dye concentration (C) in mg	0.5	1.25	2

is a powerful tool extensively used to improve the primary operating parameters impacting deterioration to establish the ideal conditions for maximal removal potential. Moreover, The statistical analysis reveals how the specified process factors interact with one another. RSM also has a model equation that links the response parameter to the control parameters. The modeling and optimization of EB dye degradation onto ZrNPs from aqueous solutions were carried out using Design-Expert software (12 versions).

A response surface model is a set of mathematical and statistical methods for determining how different parameters impact the result. [16]. RSM is used to create an analytical model for the specified purposes: examining the effects of various conditions (operational variables) and their impacts on the degradation process, identifying influential factors, and optimizing the procedure [17]. In this analysis, time (A), pH (B), and dye concentration (C) were used to determine the degradation efficiency of ZrNPs. A three-level Box-Behnken configuration was used to configure the three variables (BBD). The sample size for estimating the coefficients of a second-degree least-squares approximation polynomial is kept to a minimum. Using the BBD, the RSM is used to create an analytical model with three levels (coded as 1, 0, and +1) and 15 runs to optimize the selected variables. The concentrations and variables utilized in this analysis are listed in Table 1, following which the trials are carried out. The outcomes were assessed using analysis graphs, coefficients of determination, and analysis of variance. The result is considered significant when the P-value is less than 0.05. The obtained data were fitted to a quadratic polynomial equation for three variables as given below.

$$Y(\%) = \beta_0 + \sum_{i=1}^{3}\beta_i X_i + \sum_{i=1}^{3}\beta_{ii} X_i^2 + \sum_{i<j}\beta_{ij} X_i X_j \qquad (3)$$

where Y is the efficiency of EB dye adsorption; X_i is variables to be considered ; (β_0 . , β_i . , β_{ii} and β_{ij}) are the intercept, quadratic, linear, and interaction effects represented by the model terms.

The values of regression parameters such as the correlation coefficient R^2, modified R^2, p-value, and lack-of-fit, were determined using analysis of variance (ANOVA), which were then used to determine the validity and suitability of the predicted model. The significance of independent variables on the EB adsorption process was assessed using the 95 percent confidence level in the established model.

Statistical Error analysis

Nonlinear regression analyses of equilibrium and kinetic models were carried out using experimentally collected data. Microsoft Excel was used to compute experimental data. T experimental data were fit to the chosen models using a nonlinear least square technique utilizing SOLVER bad on the Generalized Reduced Gradient (GRG) method. The following statistical parameters were used to determine the goodness of fit: Absolute Percentage Error (APE), Sum of square error (SSE), nonlinear Chi-Square (χ2), Hybrid Fractional Error Function (HYBRID), Root Mean Square Error (RMSE), average relative error (ARE), the sum of absolute error (SAE), Akaike information criterion (AIC), Akaike information corrected criterion (AICc), Marquardt's percent standard deviation (MPSD), Nonlinear square deviation (NSD). The coefficient of determination (R^2) was also evaluated as a primary criterion. Table 2 (Equations 4–12) represents statistical parameters' mathematical expressions.

Experimental procedure for Antibacterial activity

Antibacterial activity of ZrNPs was screened against three bacterial strains, namely Gram-negative *Klebsiella pneumoniae* and Gram-positive bacteria *Bacillus subtilis* by the agar well diffusion method [18]. 100 µL of 24h mature broth culture of individual pathogenic bacterial strains were spread on the surface of nutrient agar plates using a sterilized L-shaped glass rod. Then, 6 mm wells were made in each nutrient agar plate using a sterile cork borer. The ZrNPs were dispersed in pure

Table 2. List of non-linear error functions as the statistical goodness of fit measures

Error function	Mathematical expression	ZrO_2	Equation
Coefficient of Determination (R^2)	$\frac{\sum_{i=1}^{n}(\%R_{pred}^{i}-\%R_{exp}^{i})^2}{\sum_{i=1}^{n}[(\%R_{pred}^{i}-\%R_{mean,exp}^{i})^2]}$	0.9942	4
Sum of the squares of errors (SSE)	$\sum_{i=1}^{n}\left(\%R_{pred}^{i}-\%R_{exp}^{i}\right)^2$	98.78	5
Sum of the absolute errors (SAE)	$\sum_{i=1}^{n}\left\|\%R_{pred}^{i}-\%R_{exp}^{i}\right\|$	31.26	6
Hybrid fractional error Function (HYBRID)	$\frac{100}{n-p}\sum_{i=1}^{n}\frac{\left(\%R_{pred}^{i}-\%R_{exp}^{i}\right)^2}{\%R_{exp}^{i}}$	14.42	7
Pearson's Chi-square Measure χ^2	$\sum_{i=1}^{n}\frac{\left(\%R_{pred}^{i}-\%R_{exp}^{i}\right)^2}{\%R_{exp}^{i}}$	1.955	8
Average relative errors (ARE)	$\frac{100}{p}\sum_{i=1}^{n}\frac{\left(\%R_{pred}^{i}-\%R_{exp}^{i}\right)^2}{\%R_{exp}^{i}}$	6.855	9
Absolute Percentage errors (APE)	$\frac{100}{n}\sum_{i=1}^{n}\frac{\left(\%R_{pred}^{i}-\%R_{exp}^{i}\right)^2}{\%R_{exp}^{i}}$	34.277	10
Root means square errors (RMSE)	$\sqrt{\frac{1}{n-1}\sum_{i=1}^{n}\left(\%R_{pred}^{i}-\%R_{exp}^{i}\right)^2}$	2.656	11
Marquart's percentage standard deviation (MPSD)	$100*\sqrt{\frac{1}{n-p}\sum_{i=1}^{n}\frac{\left(\%R_{pred}^{i}-\%R_{exp}^{i}\right)^2}{\%R_{exp}^{i}}}$	6.59	12

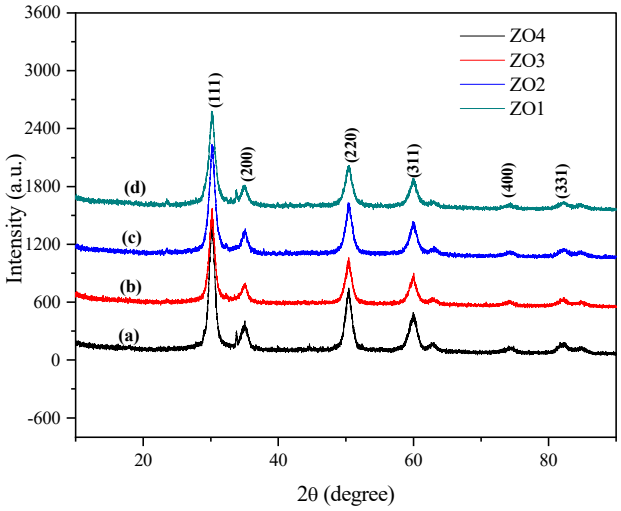

Fig. 1. (a)-(d): PXRD Pattern for ZrNPS (a) ZO1 and, (b) ZO2, (c) ZO3 and (d) ZO4 nanoparticles using Basella Alba raw juice as Natural fuel.

distilled water and different concentrations of 1000 and 1500 µg/well. Simultaneously, the standard antibiotics (ciprofloxacin used as a positive control) are tested against the pathogenic bacterial strains. The process was repeated three times and the average data were used to assess the antibacterial effect.

RESULTS AND DISCUSSIONS

PXRD Studies

The synthesized ZrNP's crystalline phase and structure were analyzed utilizing powder X-ray diffraction (PXRD). The PXRD patterns of cubic phase ZrNP with various fuel concentrations from 5 mL to 20 mL are shown in **Figs. 1(a)** to **1(d),** respectively**.** As seen in the resulting material, both monoclinic (JCPDS No. 65-1024) and cubic (JCPDS No. 49-1642) ZrO_2 are observed. The results suggest that ZrNPs demonstrate typical diffraction peaks corresponding to the (111), (200), (220), (311), (400), and (222) structure planes at 30.1^0, 34.9^0, 50.4^0, 59.9^0, 74.3^0, and 82.2^0. All curve

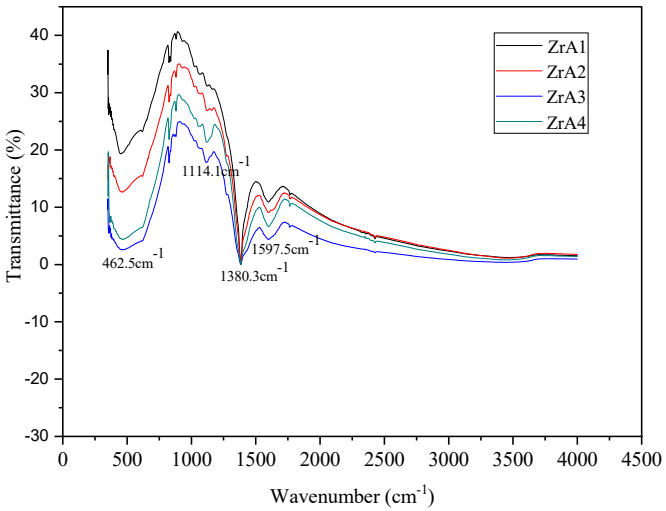

Fig. 2. (a)-(d): FTIR graphs for ZrNPS (a) ZO1 (b) ZO2 (c) ZO3 and (d) ZO4 nanoparticles

X-ray diffraction peaks are relative to the pure cubic and monoclinic ZrO_2 standard results. No extra peaks besides the cubic and monoclinic phase ZrNP suggested no impurity phases were noticed in the ZrNP obtained. While it is hard to differentiate the tetragonal and cubic phases from the XRD pattern, the cubic zirconia peak (400) did not break into two peaks that were characteristic of the cubic phase but not characteristic of the tetragonal phase. The crystallite size measured from the widening (111) plane at $2\theta = 30.1^0$ by the Scherrer formula is around 5.2nm [19,20]

FTIR Studies

The FTIR spectrum of the ZrNP was measured to determine the presence of functional groups, as shown in **Figs. 2(a) to 2(d).** The spectrum of ZrNP relies on the preparatory methods employed, the structure of the solid state, and many more. At the 473 cm^{-1} range, the intense FTIR absorption peak obtained is attributed to the Zr-O vibration, which supports the ZrO2 structure formation. The notable peak of 1380.3 cm^{-1} regions is O-H bonding, the peak of 1597.5 cm^{-1} could be attributable to the adsorbed moisture. If the material has a rough surface or comprises an inorganic composite material, the baseline of the transmission spectrum can decline off on the left. It is triggered by the dispersion of infrared light on the surface or inside of the sample and, for the lower wavelengths, this effect is stronger [21].

SEM, TEM, and EDS analyses of ZO3 nanoparticles

Scanning electronic microscopy (SEM) is one of the most common methods of characterization and is used to examine adsorbent surface properties, shapes, and morphology. **Fig. 3a** shows the morphology of the nanoparticles**,** which is mainly a cloud-like structure. They have large surfaces for the degradation of dyes. The TEM analysis was mainly analyzed to study the size, growth, and crystallites. **Fig. 3b** shows the TEM image of ZO3 nanoparticles, and the image, confirms consistent growth, and the majority of the species are well dispersed with little concentration of aggregates. The average size was calculated to be 14.7 nm. The SAED patterns in **Fig. 3c** give the well-distinct diffraction rings and were marked with the corresponding Miller indices of cubic phase ZrNP and from the SAED pattern denote the polycrystalline structure of ZO3 nanoparticles, and such findings are all in strong accordance with the results of the XRD. The elemental composition analysis of ZO3 nanoparticles was confirmed by using the energy dispersive spectroscopy (EDS) technique. The spectra authenticate the presence of Zr and O elements with a weight % of Zr are 47.62 % and O is 52.38%, as given in **Fig. 3d**. From the EDS technique, it is identified as a ZrO_2 nanoparticle.

UV-Visible and photoluminescence Studies

The UV absorbance spectrum of calcinated ZrNPs is shown in **Figs. 4(a) to 4(d).** The prominent absorption peak at 209.4 nm is because of the blue shift from the bulk ZrO_2 and characteristic of the ZrO_2 nanoparticles. Because of the transitions between the valence and conduction bands, the prominent absorption band emerges, and it

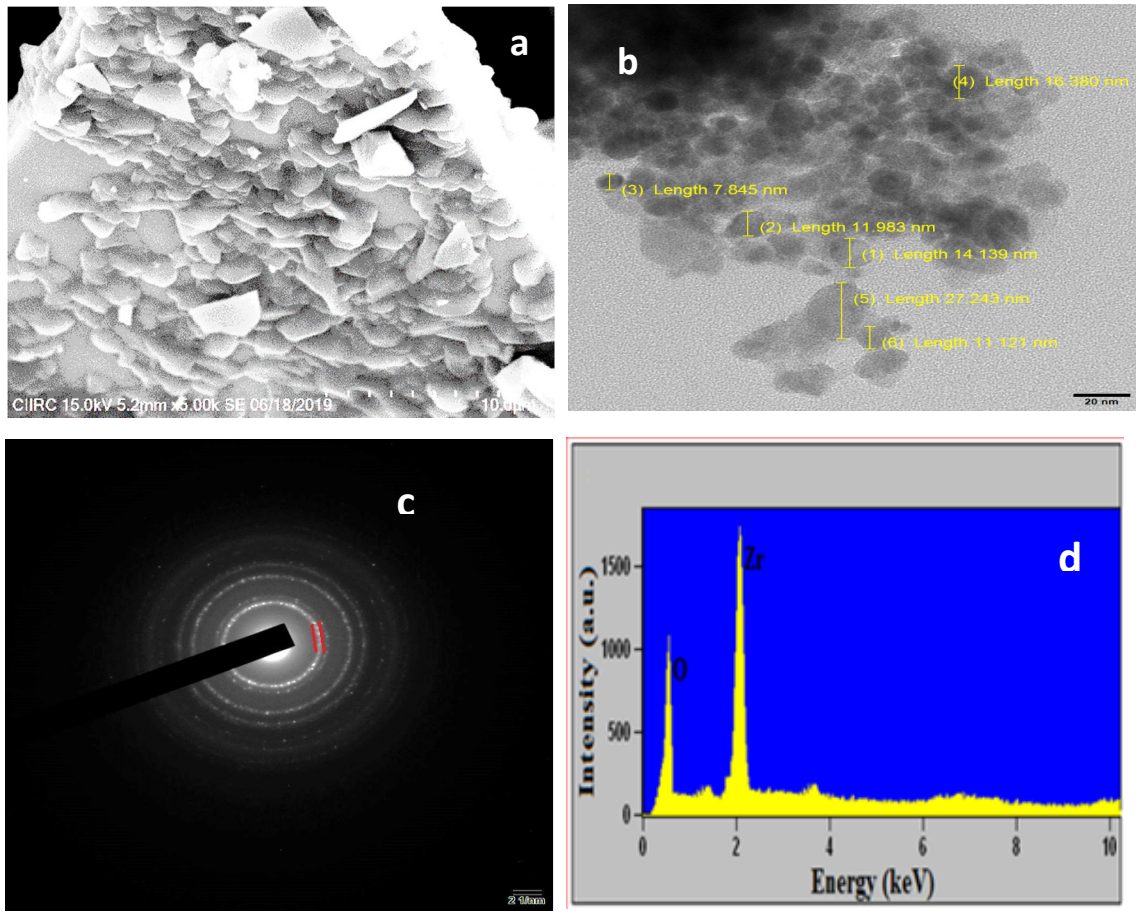

Fig. 3. (a) SEM images showing flaky surface, (b) TEM images (c) SAED pattern and (d) EDS spectrum of pure Zr, O elements

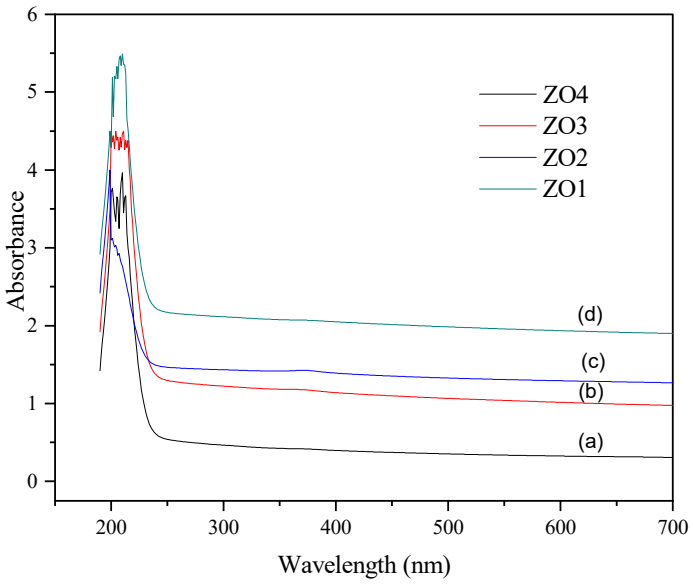

Fig. 4. UV-Vis absorption spectrum for ZrNPS (a) ZO1 (b) ZO2 (c) ZO3 and (d) ZO4 nanoparticles

Table 3. Properties like crystal size, surface area, quantum efficiency and band gap values of the prepared nanomaterials

Samples	Crystal size (nm)	BET Surface area (m^2/g)	Quantum efficiency	Bandgap energy (eV)
ZO1	28.3	45.9	0.11	5.21
ZO2	27.5	48.6	0.19	5.32
ZO3	28.6	54.7	0.28	5.14
ZO4	28.9	50.2	0.15	5.33

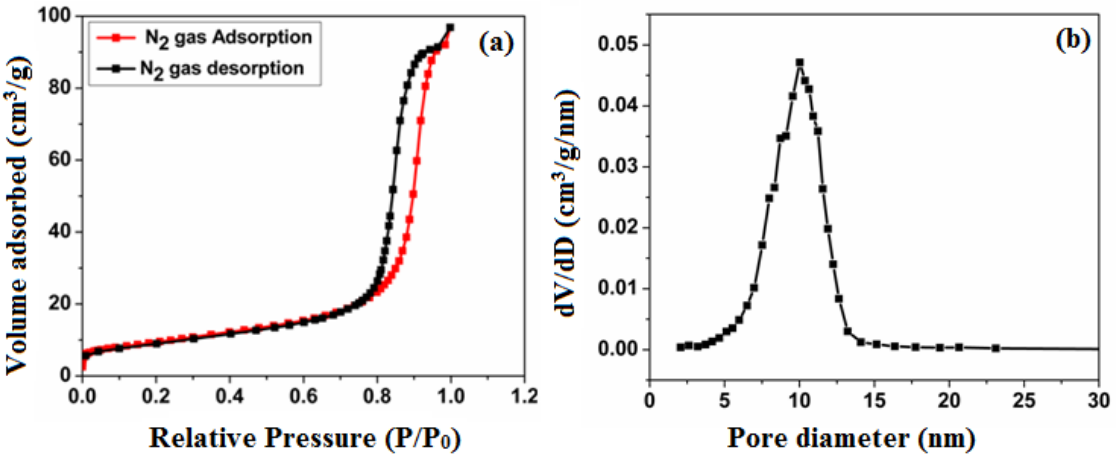

Fig. 5. (a) the BET surface area and (b) the N_2 Barret-Joyner-Halenda (BJH) pore size distribution plot of ZO3 nanoparticles.

corresponds with the published literary works of ZrO_2 nanoparticles. Usually, this greater band gap value arises with finer nano-sized particles [22].

BET surface area and pore size analyses of ZO3 nanoparticles

The cubic crystal of ZrNP was determined using the Debye-Scherrer formula. BET surface area, quantum efficiency, and the Energy of the Band Gap ZO1, ZO2, ZO3, and ZO4 nanoparticles are reported in **Table 3**. **Fig. 5(a)** to **5(d)** showed the BET surface area and the N_2 Barret-Joyner-Halenda (BJH) pore size distribution plot of ZO3 nanoparticles, respectively. adsorption-desorption isotherms exhibit a typical IUPAC type IV pattern via the existence of a hysteresis loop. BET surface area analysis was reported to be 54.7 m^2g^{-1}. Based on the BJH equation, the main pore size of our ZO3 nanoparticles is 8.8 nm. All these observational data indicate the efficient preparation of ZrO_2 nanoparticles.

Degradation of EB dye

Photocatalytic reactions were performed with the aid of 6UV-A lamps in the setup reactor. At 365 nm, the peak emission intensity was conducted. The solution of dye and catalyst was vertically irradiated. Between the source and the solution, a gap of 16 cm was fixed. At room temperature, the experiment was conducted. A 20 mL dye solution of appropriate concentrations EB (0.4 mg/L) was taken in a 100 mL beaker to study photodegradation. The effect of pH on the photodegradation of dyes was studied over a pH range from 2.0 to 12.0. The experiments were also carried out with varying amounts of catalyst from 5mg to 20.0 mg.

Comparative degradation study of ZrNPs

To compare the degradation of EB dye by ZrNPs (ZO1, ZO2, ZO3, and ZO4) synthesized by different concentrations of Basella Alba extract as fuel as shown in **Figs. 6(a) and (b).** A set of photocatalytic experiments were performed under similar conditions at a constant dye concentration and catalytic load. The figures show the variation of C/C_0 and % of the degradation rate of Evan's blue dye with time. The results illustrate that ZrNPs act as an effective photocatalyst and degrade more than 87% of dye in 60 minutes. A significant degradation capacity of ZO3 was observed and degraded 93.37% of the dye in 60 minutes. Among ZrNPs, the ZO3 compound has a very high photodegrade potential rate, and ZO4 has the lowest and degrades 87.30% of dye in the same period. Though dye is the same for ZrNPs, degradation is more on ZO3. Further comparing the degradation of

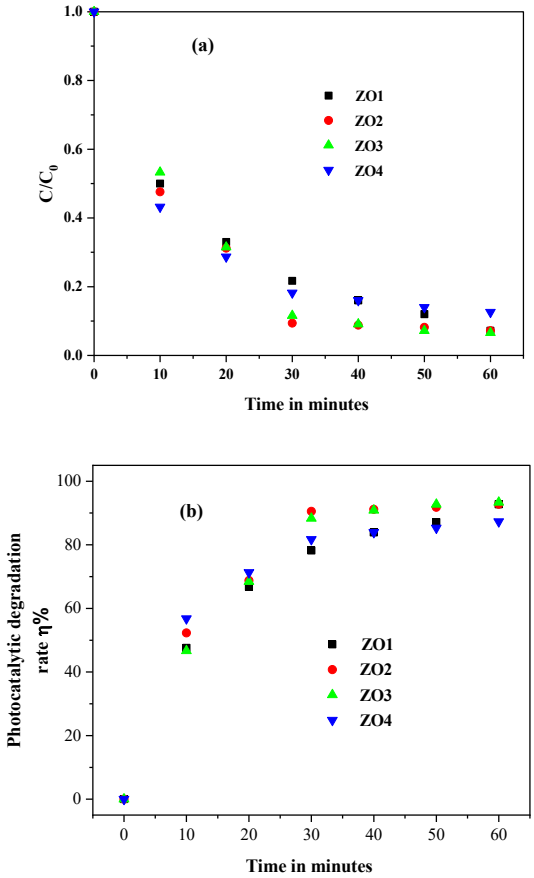

Fig. 6. (a) and (b) photo catalytic properties of ZO series compounds on EB dye by keeping the amount of catalyst (0.010 g/L), concentration of dye (0.40 mg/L) and time of irradiation constant

EB dye by ZrNPs (ZO1, ZO2, ZO3, and ZO4), it was clear that ZO3 nanoparticles showed better degradation of dye than ZO1, ZO2, and ZO4 nanoparticles, the increased photocatalytic activity of ZO3 nanoparticles due to its highest surface area and porous nature. One of several essential key factors influencing photocatalytic behavior is the surface area of a photocatalyst. Among the different catalysts (ZO1, ZO2, ZO3, and ZO4 nanoparticles), ZO3 nanoparticles displayed the highest surface area and quantum yield than the other photocatalyst studies. Another reason for the increased photocatalytic activity of ZO3 nanoparticles is due to it's the intrinsic defects of ZO3 nanocrystals. The predominant defects in the ZO3 nanocrystals are positively charged Zr interstitials and oxygen vacancies. When light irradiation takes place, electron-hole pairs are formed, the Zr interstitials and oxygen vacancy created by Oxygen facilitate redox reactions by trapping photo-generated electrons, which decreases the conjugation of electrons and holes, and they are obtained for dye degradation [23] and thus resulting in increased degradation of EB dye.

Mechanism of dye degradation(see also Scheme 3) [24–26]

$$ZrO_2 + hv \rightarrow h^+ + e$$

$$e + O_2 \rightarrow O_2^{\cdot}$$

$$O_2^{\cdot} + EB\,dye \rightarrow CO_2 + H_2O$$

$$h^+ + EB\,dye \rightarrow CO_2 + H_2O$$

$$h^+ + H_2O \rightarrow {\cdot}OH + H$$

$${\cdot}OH + pollutant \rightarrow CO_2 + H_2O$$

Effect of controlling parameters on Dye Degradation.

RSM was used to evaluate the correlation and optimization of process variables, as previously

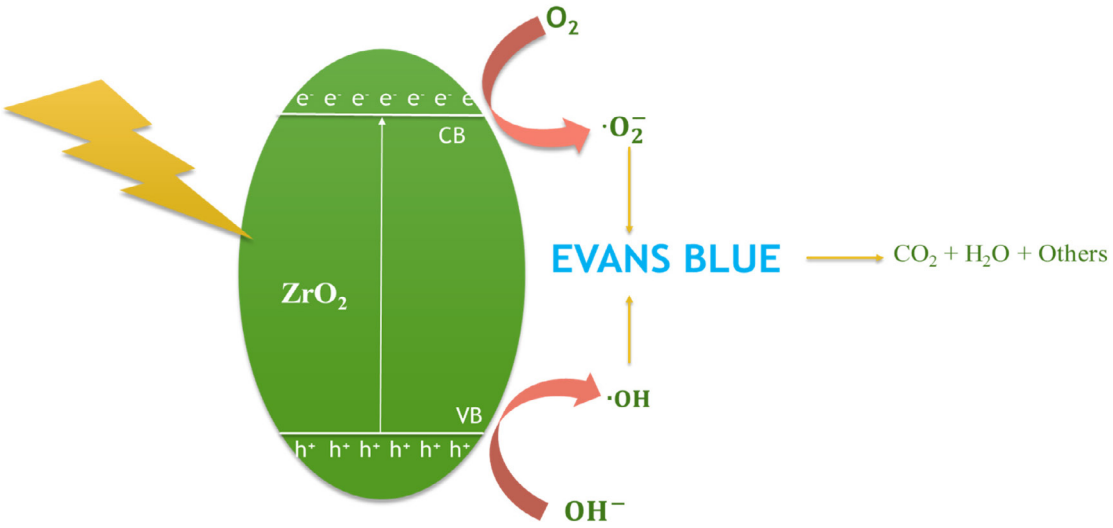

Scheme.3. The scheme for the degradation mechanism of ZrNP

Table 4. BBD matrix of variables along with actual, fits, and residual values for adsorption of EB on ZrO_2

Trial No.	A	B	C	Experimental value of % Degradation	Predicted value of % Degradation	Residual Removal
1	0	1	-1	97.1	94.3625	7.49
2	-1	0	-1	20.5	18.525	3.90
3	1	0	-1	92.4	93.65	1.5625
4	1	-1	0	93.7	88.9875	22.207656
5	1	1	0	99.8	101.288	2.214144
6	-1	1	0	28.3	33.0125	22.207656
7	1	0	1	83.6	85.575	3.900625
8	0	1	1	87.7	84.23	12.0409
9	0	-1	1	71.3	74.03	7.4529
10	0	0	0	76.8	76.8	0
11	0	0	0	76.8	76.8	0
12	0	-1	-1	69.7	73.1625	11.988906
13	0	0	0	76.8	76.8	0
14	-1	0	1	18.6	17.35	1.5625
15	-1	-1	0	15.4	13.9	2.25

mentioned. The Box-Behnken model was used to develop a total of 15 experimental trials using Design-Expert tools by taking 3 center points. The BBD design matrix along with experimental and predicted values are given in Table 4. The statistical relationship between the variables and the response, which is the amount of dye adsorbed per unit mass of both the adsorbents(mgg^{-1}), is expressed with coded values (A, B, and C) as given in equation 13 depending on the response obtained from ZrO_2.

$$Y_{ZrO_2} = 76.8 + 35.8375 * A + 7.85 * B - 2.3125 * C - 1.7 * AB - 1.725 * AC - 2.75 * BC - 22.5875 * A^2 + 5.0875 * B^2 - 0.4375 * C^2$$

The significance of the major influencing of variables on the degradation process was determined by analysis of variance (ANOVA) of the regression model. Table 5 shows the results of the ANOVA for the obtained quadratic equation. The ANOVA indicates that the correlation between the response and the significant variables given in the equation is appropriate. The quadratic model was observed as being the most appropriate for the adsorption of EB. The significance of the coefficient terms is determined by the F and p-value, smaller p-value and larger F value indicate that the regression equation will explain the major

Table 5. shows the results of the ANOVA for the obtained quadratic equation

Source	ZrO_2		
	F-value	p-value	Significance
Model	72.72	< 0.0001	Significant
A-Time	520.33	< 0.0001	Significant
B-pH	24.97	0.0041	Significant
C-Dye Concn	2.17	0.2010	
AB	0.5854	0.4787	
AC	0.6028	0.4726	
BC	1.53	0.2708	
A^2	95.40	0.0002	Significant
B^2	4.84	0.0791	
C^2	0.0358	0.8574	

variations in the response. If the measured p values are less than 0.05 then the model is considered to be statistically significant. The ANOVA analysis for the removal of MB reports that the F value for ZrO_2 is 72.72. There is only a 0.01% chance that an F-value this large could occur due to noise. From equation 13, The model parameters of Y_{ZrO_2}, i.e. A, B, B^2 are the model terms that are considered to be significant for a response. The coefficient of determination (R^2) was also used to analyze the results. The Predicted R^2 of 0.8787 is in reasonable agreement with the Adjusted R^2 of 0.9788with a difference of less than 0.2. The linear and non-linear correlation between experimental and predicted degradation % is shown in Figures 7 a-b. The non-linear graph shows a good relationship between the experimental and predicted values and the data points were well distributed close to a straight line in the linear graph with R^2 values of 0.9912 for ZrO_2. The results also show that the chosen quadratic model is adequate for the removal of EB by ZrO_2 [24,25].

Even though predicted values match the experimental results better, it does not provide statistical significance and error distribution. As a result, to further validate the effectiveness of these methods, their efficiency is statistically evaluated using well-established statistical metrics. Normally, the accuracy of the prediction is determined by calculating the correlation coefficient and fitting a straight line. This method explains the strength and direction of linear relationships between experimental and model predictions, but it does not fully reflect nonlinear relationships in the error distribution. The R^2 values for the experimental and predictions by RSM for ZrO_2 are 0.9942, implying that the proposed models given are very similar to experimental values. ARE was calculated to be 6.85549, whereas the APE was estimated to be 34.27745. The RMSE was calculated to be 2.656291, indicating that the error deviation is significantly lower than predicted by RSM. The other metrics HYBRID and MPSD are also significant for RSM and Pearson's Chi-square measure offers a convenient measurement scale for weighing the goodness of fit is found to be 1.955787.

Three-Dimensional Response Surface and Two-Dimensional Contour Plot

To evaluate the individual and relative impact of these variables on the response and to find the optimal value, 3D response surface plots and 2D contour plots were implemented. All of the processing parameters, such as time, pH, and dye concentration, have a different effect on the adsorption ability of ZrO_2. The Contact time is used to calculate the amount of interaction between the adsorbate and the adsorbent. The maximum Removal efficiency of 99.8% is observed with the given variables at a time of 60 minutes, pH at 12.0, and 2mg/L of Dye concentration. Owing to the attraction of charged dyes onto the surface of the adsorbent, pH plays an important role in dye degradation. The initial dye concentration has a major effect on the aqueous-solid phase mass-transfer resistance. The relative influence of time, pH, and dye concentration on the removal percentage of EB are shown in Figure 8 in 3D surface and contour plots.

The graph Figures 8 a and b show the impact of pH and time on dye removal by ZrO_2 with the dye concentration set to zero (Dye conc 1.25 mg/L). It was obvious that increasing the pH would aid dye removal. In the pH range of 10-12, the maximum dye removal was observed. The pH is the most significant factor which can affect the degradation

process of dye on the surface of the photocatalyst. The effects of different pH values from 2.0 to 12.0 on the degradation efficiency of dye were studied. The surface properties of ZrO_2 nanoparticles, where they impaired the dissolution of dye molecules, were modified by the pH alterations. Perhydroxyl radicals were generated, which resulted in the creation of hydrogen peroxide and hydroxyl radicals. Higher degradation efficiency in the basic medium due to an increase in positive charge on the surface of ZrO_2 catalyst and the electrostatic interaction enhances the adsorption property, thereby increasing the degradation efficiencies. Further, the hydroxyl ions available at higher pH were more, which forms more hydroxyl radicals, hence, increasing the degradation efficiency. As the contact time between the catalyst surface and the dye was increased from 05 to 60 minutes and observed a rapid increase initially from 5 minutes to 30 minutes because of the less turbidity but from 30 to 60 minutes there is a steady increase due to the turbidity of the solution. The response surface plot for ZrO_2 revealed a distinct elevation, and the subsequent contour plot revealed a diagonally elongated uniform pattern, meaning that the interaction between pH and time had a major impact on dye degradation. [26].

Figure 8 c and d demonstrate the cumulative influence of Time and Dye concentration on dye removal when the pH is set to zero (pH, 7.0). The degradation efficiency (Y) increases with a minimum difference as the dye concentration is increased from 0.5 to 2 mg/L, and achieves its maximum value, which is mostly dependent on the Time of Contact. When the contact period between the catalyst surface and the dye was increased from 30 to 60 minutes, the removal efficiency improved. The response surface plot displayed a prominent peak, and the contour plot had an elongated pattern, showing that dye concentration and time had a substantial mutual interaction. However, when the amount of catalyst exceeds 20 mg, the turbidity of the suspension increases, which decreases the penetration of sunlight and reduces the photoactivation potential of the suspension. Hence high concentrations of the catalyst may not be useful because of aggregation and light scattering [27].

While the time was set to zero (Time 32.5 minutes), Figures 8 e and f depicted the interrelationship of dye concentration and pH. Dye degradation capacity can be improved by increasing dye concentration and pH. Nevertheless, the estimated 55% degradation will be reached by pH 7.0. The elevated degradation % can be observed from pH 7.0 to 12.0. When both of these variables are increased for a long time, the dye degradation performance deteriorates. This is most likely owing to a scarcity of potential binding sites. The response surface plot revealed an elevated graph for both the adsorbent, while the contour plot revealed a distinctive -green-colored elongated pattern, implying that the dye concentration and pH interaction had a major impact on dye removal.

Optimization is used in any method of multiple responses to achieve the desired relevant variables being evaluated at the same time. Maximum response with Time, pH, and Dye concentration were selected as constraints. Under the constraints, the optimum conditions for EB removal are 1.25mg/L dye concentration at pH 12.0 and a contact time of 60 minutes, with a response of 99.8 % which shows that green synthesized ZrO_2 nanoparticles are highly efficient in dye degradation compared to previously reported studies as reported in Table 6.

Effect of controlling parameters individually

Effect of dye concentration

The influence of dye concentration on the degradation of EB dye was examined using ZO3 nanoparticles prepared by Basella Alba extract as fuel, as shown in **Fig. 9a.** The catalyst concentration

Table 6. Comparison on Degradation capacity of ZrO_2 based nanocomposite

Sl. No.	Material	Dyes	Light source	Duration in minutes	Degradation in %	Reference
1	ZrO_2-TiO_2	AB, RBBR, and ACG	UV	120	100	[1]
2	t-ZrO_2	MO	UV	50	99	[2]
3	TiO_2 - ZrO_2	TOC	UV	90	90	[3]
4	ZrO_2 doped lead oxide	RhB	UV	180	93.32	[4]
5	Ti_8Zr_2	RhB	UV	90	96.8	[5]
			Our report			
	Green synthesized ZrO_2	**EB**	**Visible**	**60**	**99.8**	

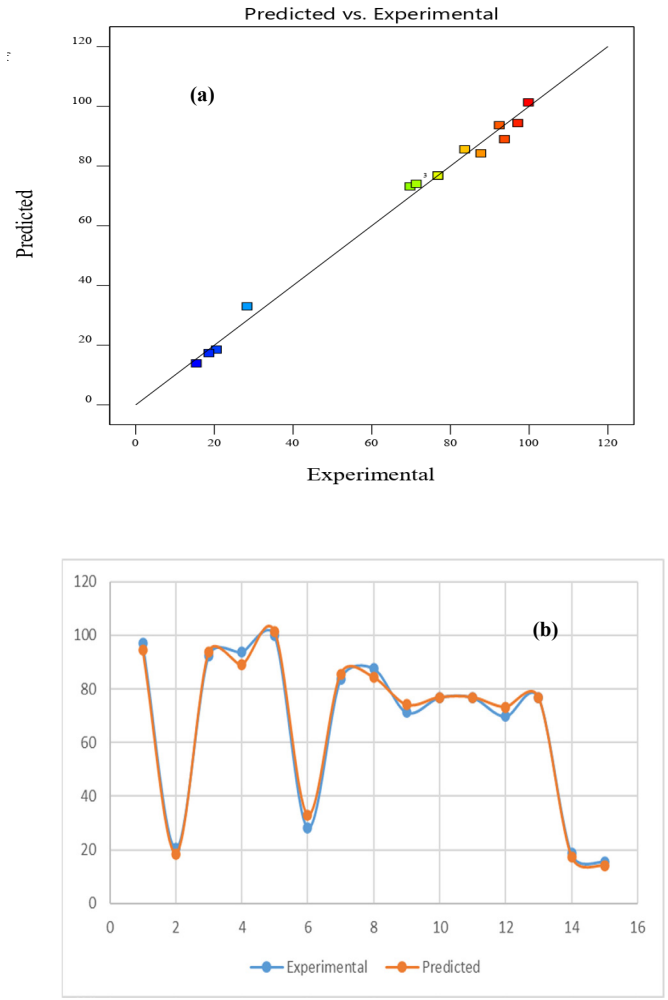

Fig. 7. (a) Linear and (b) Non-Linear correlation between experimental and predicted Degradation % on ZrO2

was kept constant at 0.075g/L, and the dye concentration varied from 0.5 to 8 mg/L. Below the optimal load, increased active sites on the catalyst surface resulted in rapid degradation. The turbidity of the slurry rises beyond the optimum level, thus decreasing light penetration, which reduces the supply of hydroxides and superoxides [28]. As the concentration of the dye increases, the time required for complete degradation also increases. Several dye molecules were adsorbed in greater levels on the catalyst surface, contributing to a reduction in the number of active sites [smaller value of hydroxyl and superoxide radicals], which decreases light exposure & the impact of pH on dye solution degradation.

Effect of pH

As given in **Fig. 9b** The pH of the solution was adjusted [0.01 M NaOH or 0.01 M H_2SO_4], and the efficiency of degradation was studied. The surface properties of ZO3 nanoparticles, where they impaired the dissolution of dye molecules, were modified by the pH alterations. Perhydroxyl radicals were generated, which resulted in the creation of hydroxyl radicals and hydrogen peroxide. The maximum degradation was shown by ZO3 nanoparticles at pH 6, which was in clear compliance with earlier reports [26].

The pH is the significant factor that can influence the degradation of dye on the photocatalyst surface. The impacts of various pH levels from 2.0 to 12.0 on the degradation efficiency of dye were studied. In the basic medium, the degrading efficiency of EB was found to be high. The degradation efficiency of EB was found to be more than 82.05% in the first 20 minutes and reaching 100 % in 60 minutes

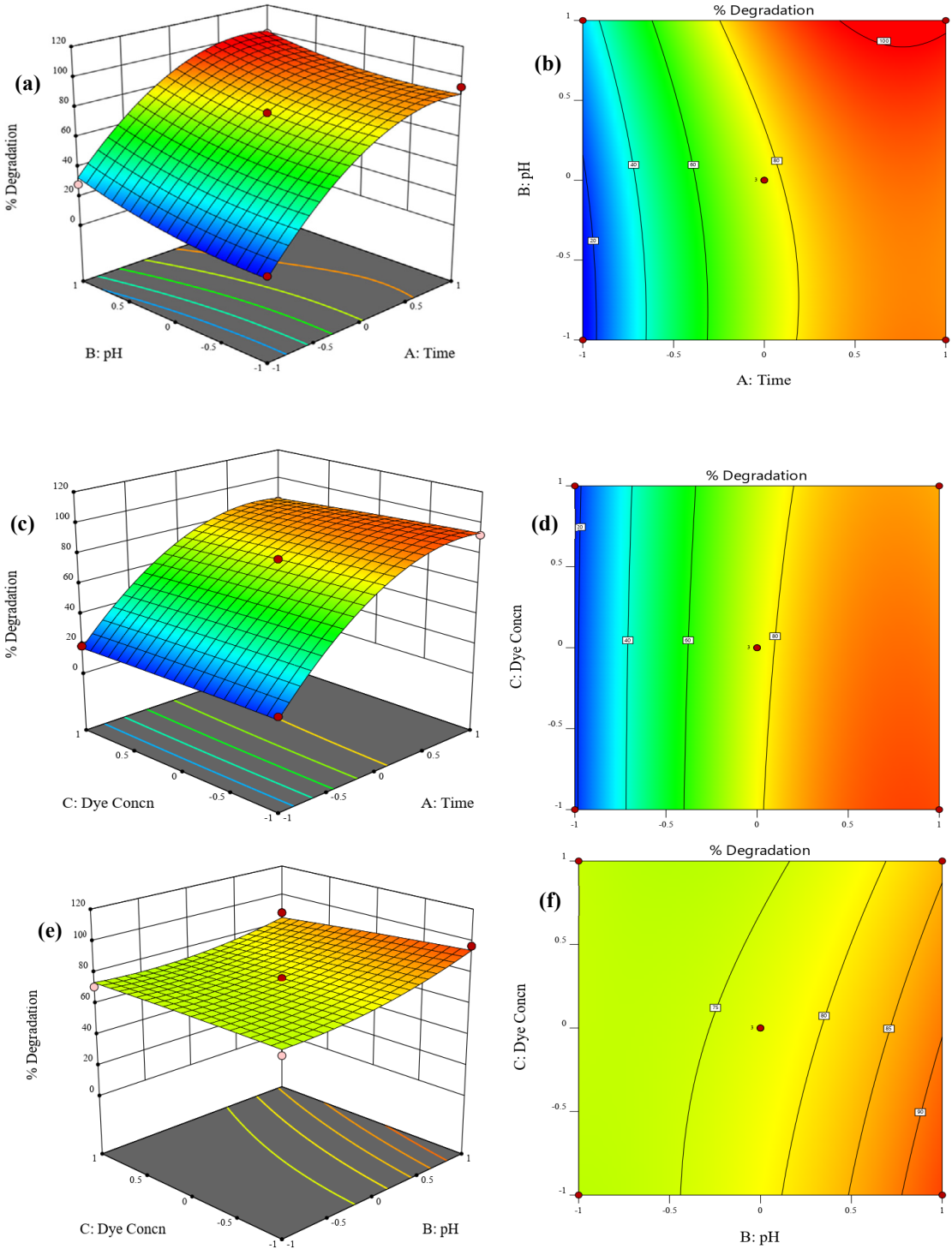

Fig. 8. (a) and (b) the cumulative impact of pH and time, (c) and (d) the cumulative impact of time and Dye concentration and (e) and (f) the cumulative impact of pH and Dye concentration on dye degradation

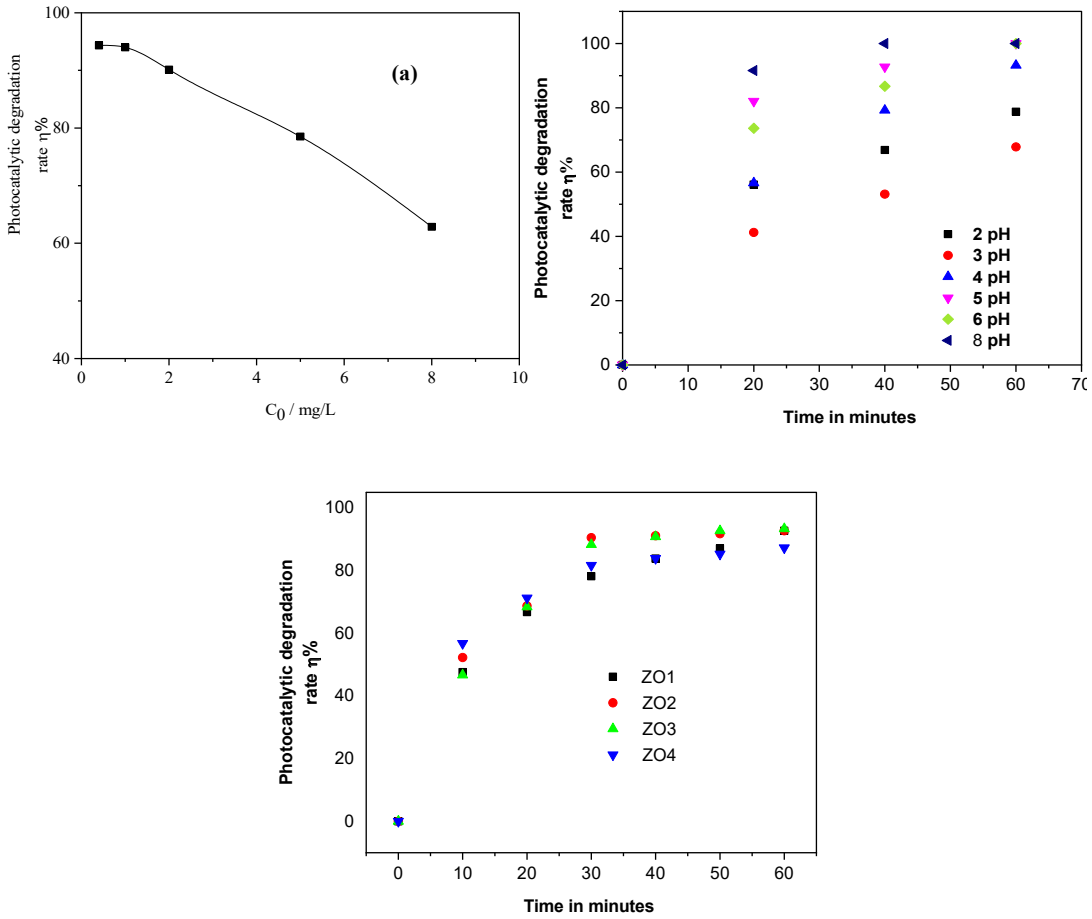

Fig. 9. a) Effect of dye concentration, b) Effect of pH (catalyst concentration kept constant at 0.075g/L, and the dye concentration was varied from 0.5 to 8 mg/L), and c) Effect of catalyst concentration (different concentrations of ZrNPS from 05 mg to 20 mg at a constant dye concentration of 0.4 mgL^{-1})

at pH 10.0., whereas 100% degradation of EB was observed in less than 40 minutes at pH 12.0. The increased positive charge on the surface of the ZO3 catalyst leads to improved degrading efficiency in the basic medium and the electrostatic interaction enhances the adsorption property, thereby increasing the degradation efficiencies. Further, the hydroxyl ions available at higher pH were more, which forms more hydroxyl radicals, hence, increasing the degradation efficiency.

Effect of catalyst concentration

Under the same circumstances and with varying concentrations of ZrNPs (ZrNPs from 05 mg to 20 mg at a constant dye concentration of 0.4 mgL^{-1}), the effect of ZrNPs on Evans Blue degradation was evaluated. **Fig. 9c** illustrates that there is no significant change in degradation efficiency with the increase in the concentration of catalyst from 05 mg to 15 mg, and afterward, the rate of degradation remains nearly constant. However, when the amount of catalyst exceeds 20 mg, the turbidity of the suspension increases, which decreases the penetration of sunlight and reduces the photoactivation potential of the suspension. Hence high concentrations of the catalyst may not be useful because of aggregation and light scattering.

Photocatalytic activity of the recycled catalyst

To check the reusability of the photocatalyst after the first application, ZO3 nanoparticles were collected, then washed twice and dried for two hours at 80 °C. The dried ZO3 nanoparticles have been used again for almost four cycles as a photocatalyst to degrade the dye. The stability of the photocatalyst ZO3 was assessed by using the catalyst for three photodegradation experiments

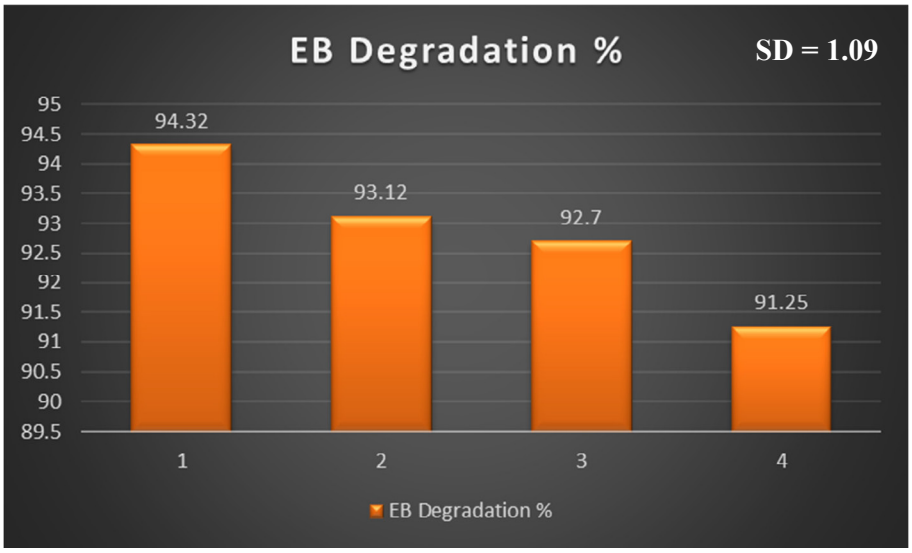

Fig. 10. Effect of reusability and photostability test of ZO3 nanoparticle on photocatalytic degradation of dye.

by keeping the same concentration of EB dye. After each degradation process, Deionized water was used to wash the catalyst and alcohol to remove any adsorbed EB on the surface and then dried in the oven. After four cycles, the photocatalyst showed remarkable stability, with an EB degradation of 91.25 %, as given in **Fig. 10**. The loss of the photocatalyst owing to washing in between cycles could be responsible for the drop in degrading efficiency. The photocatalyst's stability means that it can be reused several times, lowering effluent treatment expenses. The slight reduction in catalytic properties possibly leads to the accumulation and sedimentation of the dye on the nanoparticle of ZO3, making portions of the surface of the catalyst unavailable for dye adsorption and hence photon adsorption, reducing the efficiency of the catalytic reaction. This became obvious, according to the above study, that the photocatalyst ZO3 showed strong photostability.

Antibacterial activity Studies

The antimicrobial effect of ZO3 nanoparticles with different concentrations was studied using a well-diffusion assay against the gram-positive bacterium *Bacillus subtilis* and the gram-negative bacterium *Klebsiella pneumoniae*. Each of the Petri plates containing autoclaved, solid Mueller Hinton agar (Hi-media Laboratories, India) was inoculated with respective bacterial strains. 100µL of these organisms were spread using a sterile L-shaped glass spreader with 24 hrs mature broth culture containing 10^6 colonies forming units (CFU). Immediately after spreading the bacterial cultures, a sterilized cork borer was used to bore well-like standardized holes. Aseptically, various concentrations of ZO3 nanoparticles were synthesized (50, 25, 12.5, and 6.25 mg/mL got by serial dilution of the sample) and incorporated into these wells to assess the antibacterial activities. ZO3 nanoparticles were distributed in sterile water, and no negative controls were used because the chemicals were used in such low quantities. Each concentration was added inside the well at the volume of 100µL, which was previously inoculated with different bacterial strains. As a negative control, autoclaved distilled water was taken, and the Gentamicin antibiotic disc was used as a positive control (Hi-Media, Mumbai, India). Eventually, these plates are aerobically incubated in a bacteriological incubator at 37 °C. The discrepancy between both the overall inhibition zone diameter as well as the good diameter after 24 hours of incubation was measured as the Zone of Inhibition (ZOI). Tabulation of the result is given in **Table 7** and **Fig. 11,** for the zone inhibition measured in millimeters for all the plates. **Fig. 12** shows the photographs of the antibacterial activity of ZO3 nanoparticles in the zone of inhibition method against the gram-positive bacterium *Bacillus subtilis* and the gram-negative bacterium

Klebsiella pneumoniae [29,30].

When the concentration of ZrNPs increases, the

Table 7. Tabulation of the results for the zone inhibition measured in millimetre

Antimicrobial activity of ZO3 nanoparticles			
Group	Treatment	Zone of inhibition of radius in mm	
		Bacillus subtilis (Gram Positive)	*Klebsiella pneumoniae* (Gram Negative)
1	ZO3 (50mg/100µL)(***)	10±0.3	0.3
2	ZO3 (25mg/100µL)(**)	2.4±0.5	0.1
3	ZO3 (12.5mg/100µL)	0.7±0.3	Not seen
4	ZO3 (6.25mg/100µL)	0.3	Not seen

Values represent the Mean SE for n=3 replicates. [**] p<0.01, [***] p<0.01 as compared from Gram +ve to Gram -ve bacteria.

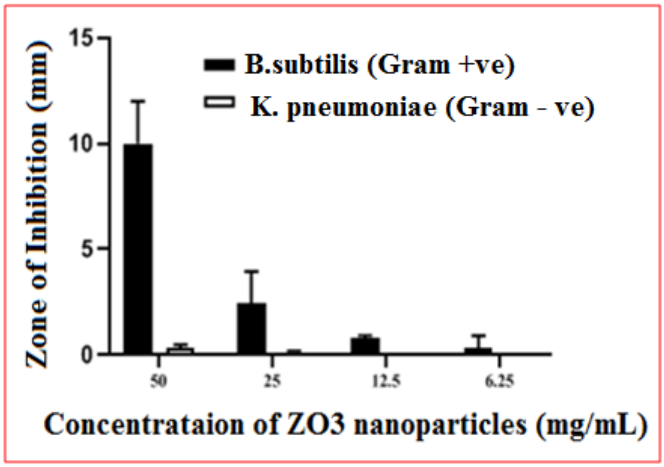

Fig. 11. The zone inhibition measured plot of different concentrations of ZO3 nanoparticles.

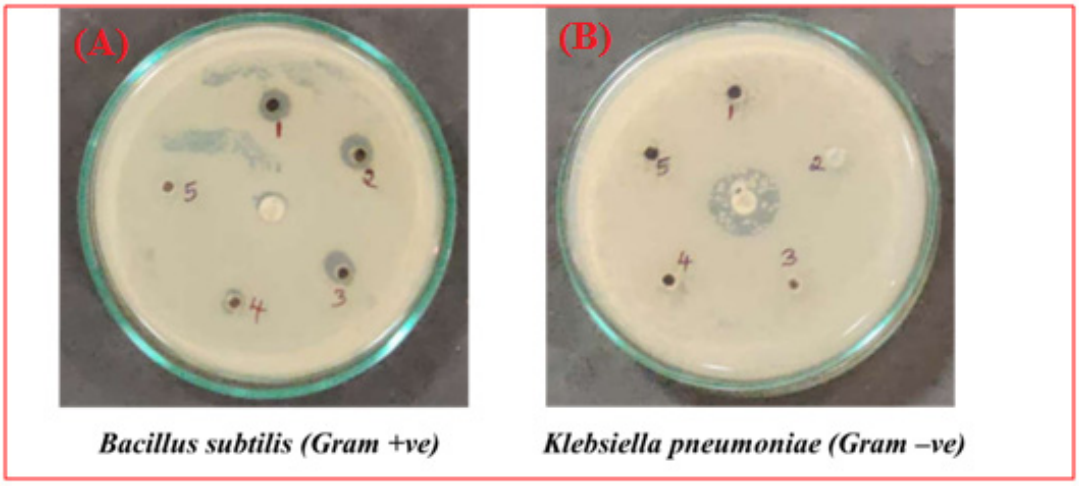

Fig. 12. Antibacterial activity of ZO3 nanoparticles using the agar well diffusion method. A- *Bacillus subtilisand* B- *Klebsiella. pneumoniae*. ZO3 nanoparticles were diluted at the concentrations 1: 50mg/ml; 2: 25mg/ml; 3: 12.5mg/ml, 4: 6.25mg/ml, 5: Sterilised water and center will be Gentamicin (antibiotic), wells werefilled with 25µl of the sample.

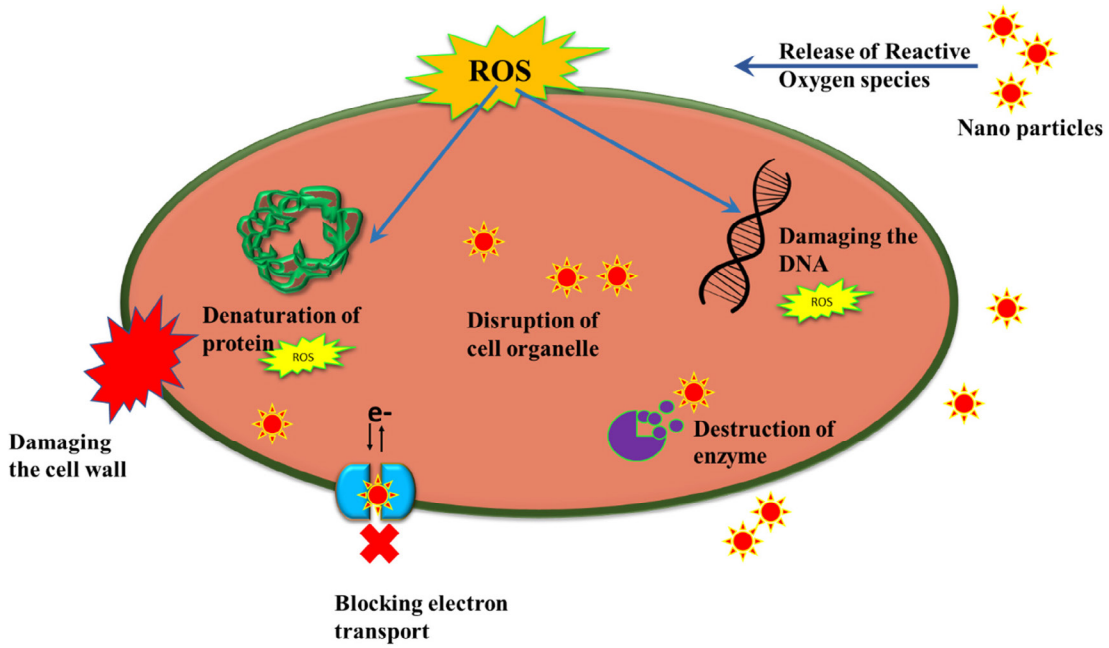

Scheme.4. The scheme for the antibacterial activity of ZrNP

growth of microbiological strains is significantly hampered. The capacity of ZrNPs composites to attach to bacteria due to their opposing electric charges, which lead to a decrease in the bacterial cell wall, is largely responsible for their antibacterial properties[31]. Gram-negative bacteria had a stronger interaction with nanoparticle composites than Gram-positive bacteria, owing to variations in cell walls, cell structure, physiology, metabolism, or degree of contact of organisms with nanoparticles. The peptidoglycan cell walls of Gram-positive bacteria are thicker than those of Gram-negative bacteria, making nanoparticle composites more difficult to enter. As a result, the antimicrobial response is comparatively less[32]. Because of their structural and physiochemical properties, nanomaterials induce oxidative stress as a primary antibacterial mechanism. Direct interaction of ZrO_2 with bacterial cell walls, on the other hand, has been shown to result in the breakdown of bacterial cell integrity, the release of antimicrobial ions, particularly Zr^{2+} ions, and the formation of reactive oxygen species (ROS)[31,33,34]. The remarkable antibacterial activity of ZrNPs is assumed to be due to the greater surface area of smaller nanoparticles and ROS production [35,36]. The antibacterial action mechanism is depicted in Scheme 4.

CONCLUSIONS

In the current work, the solution combustion process reported the synthesis of ZrNP with a tetragonal crystal structure using Zirconium (IV) oxynitratehydrate as the metal precursor and an oxidizer, Basella alba raw extract as natural fuel at 600°C. Natural fuel is utilized to avoid harmful chemical fuels, which may pollute the environment during combustion. The influence of nanocrystalline zirconia particles on this framework and the composition of the fuel-to-oxidant molar ratio have been examined. The Physiochemical properties of the ZrNPs were analyzed through characterization tools. The effect of catalytic load, pH, light sources, dye concentration, and reusability of the ZrNPs on the degradation activity of EB has been studied thoroughly. By taking three center points, 15 experimental trials were created utilizing the Box-Behnken model-RSM. The maximum Removal efficiency of 99.8% is observed with the given variables at a time of 60 minutes, pH at 12.0, and 2mg/L of Dye concentration. There is no significant difference between the linear and non-linear relationships between experimental and predicted degradation percentages. To further justify its use, the efficacy of these approaches is statistically assessed using well-established statistical criteria.

ZrNPs also exhibit good antibacterial activity against the gram-positive bacterium *Bacillus subtilis* and the gram-negative bacterium *Klebsiella pneumoniae*. The obtained results show that the ZrNPs are efficient in pollutant removal and can be further optimized for industrial scale and can also pave the way for eco-friendly synthesis of nanoparticles.

CONFLICT OF INTEREST

The authors declare that there are no conflicts of interest regarding the publication of this manuscript.

REFERENCE

[1] V.G. KERAMIDAS, W.B. WHITE, Raman Scattering Study of the Crystallization and Phase Transformations of ZrO2, Journal of the American Ceramic Society. 57 (1974) 22-24. https://doi.org/10.1111/j.1151-2916.1974.tb11355.x

[2] D.K. Smith, W. Newkirk, The crystal structure of baddeleyite (monoclinic ZrO 2) and its relation to the polymorphism of ZrO 2 , Acta Crystallographica. 18 (1965) 983-991. https://doi.org/10.1107/S0365110X65002402

[3] R. Zhang, H. Liu, D. He, Pure monoclinic ZrO 2 prepared by hydrothermal method for isosynthesis, Catalysis Communications. 26 (2012) 244-247. https://doi.org/10.1016/j.catcom.2012.06.005

[4] M.K. Musembi, F.B. Dejene, Investigation of the effect of precursor ratios on the solution combustion synthesis of zinc zirconate nanocomposite, Heliyon. 5 (2019) e03028. https://doi.org/10.1016/j.heliyon.2019.e03028

[5] A. Hirvonen, R. Nowak, Y. Yamamoto, T. Sekino, K. Niihara, Fabrication, structure, mechanical and thermal properties of zirconia-based ceramic nanocomposites, J Eur Ceram Soc. 26 (2006) 1497-1505. https://doi.org/10.1016/j.jeurceramsoc.2005.03.232

[6] W.A. Jagadish chanra Ray, Dong-Wha Park, Chemical synthesis of stabilied nanocrystalline zirconia powders, (2005) 142-148.

[7] E.C. Subbarao, H.S. Maiti, K.K. Srivastava, Martensitic transformation in zirconia, Physica Status Solidi (a). 21 (1974) 9-40. https://doi.org/10.1002/pssa.2210210102

[8] D. He, Y. Ding, H. Luo, C. Li, Effects of zirconia phase on the synthesis of higher alcohols over zirconia and modified zirconia, Journal of Molecular Catalysis A: Chemical. 208 (2004) 267-271. https://doi.org/10.1016/S1381-1169(03)00542-9

[9] T. Chraska, A.H. King, C.C. Berndt, On the size-dependent phase transformation in nanoparticulate zirconia, Materials Science and Engineering A. 286 (2000) 169-178. https://doi.org/10.1016/S0921-5093(00)00625-0

[10] W. Nimmo, D. Hind, N.J. Ali, E. Hampartsoumian, S.J. Milne, The production of ultrafine zirconium oxide powders by spray pyrolysis, Journal of Materials Science. 37 (2002) 3381-3387. https://doi.org/10.1023/A:1016549325319

[11] R.A. Espinoza-González, D.E. Diaz-Droguett, J.I. Avila, C.A. Gonzalez-Fuentes, V.M. Fuenzalida, Hydrothermal growth of zirconia nanobars on zirconium oxide, Materials Letters. 65 (2011) 2121-2123. https://doi.org/10.1016/j.matlet.2011.04.056

[12] A. Precious Ayanwale, S.Y. Reyes-López, ZrO2-ZnO Nanoparticles as Antibacterial Agents, ACS Omega. 4 (2019) 19216-19224. https://doi.org/10.1021/acsomega.9b02527

[13] T.T. Nguyen, S.N. Nam, J. Son, J. Oh, Tungsten Trioxide (WO3)-assisted Photocatalytic Degradation of Amoxicillin by Simulated Solar Irradiation, Scientific Reports. 9 (2019) 1-18. https://doi.org/10.1038/s41598-019-45644-8

[14] V. Bhatia, A. Dhir, A.K. Ray, Photocatalytic degradation of atenolol with graphene oxide/zinc oxide composite: Optimization of process parameters using statistical method, Journal of Photochemistry and Photobiology A: Chemistry. 409 (2021) 113136. https://doi.org/10.1016/j.jphotochem.2021.113136

[15] I.K. Konstantinou, T.A. Albanis, TiO2-assisted photocatalytic degradation of azo dyes in aqueous solution: Kinetic and mechanistic investigations: A review, Applied Catalysis B: Environmental. 49 (2004) 1-14. https://doi.org/10.1016/j.apcatb.2003.11.010

[16] A.R. Amani-Ghadim, S. Aber, A. Olad, H. Ashassi-Sorkhabi, Optimization of electrocoagulation process for removal of an azo dye using response surface methodology and investigation on the occurrence of destructive side reactions, Chemical Engineering and Processing: Process Intensification. 64 (2013) 68-78. https://doi.org/10.1016/j.cep.2012.10.012. https://doi.org/10.1016/j.cep.2012.10.012

[17] F. Khodam, Z. Rezvani, A.R. Amani-Ghadim, Enhanced adsorption of Acid Red 14 by co-assembled LDH/MWCNTs nanohybrid: Optimization, kinetic and isotherm, Journal of Industrial and Engineering Chemistry. 21 (2015) 1286-1294. https://doi.org/10.1016/j.jiec.2014.06.002

[18] J.M. Guerreiro Tanomaru, I. Storto, G.F. da Silva, R. Bosso, B.C. Costa, M.I.B. Bernardi, M. Tanomaru-Filho, Radiopacity, pH and antimicrobial activity of Portland cement associated with micro- and nanoparticles of zirconium oxide and niobium oxide, Dental Materials Journal. 33 (2014) 466-470. https://doi.org/10.4012/dmj.2013-328

[19] F. Shi, Y. Li, H. Wang, Q. Zhang, Fabrication of well-dispersive yttrium-stabilized cubic zirconia nanoparticles via vapor phase hydrolysis, Progress in Natural Science: Materials International. 22 (2012) 15-20. https://doi.org/10.1016/j.pnsc.2011.12.003

[20] S.B. Deshmukh, Comparative studies and gas sensing performance of bulk ZrO 2 thick and nanostructured ZrO 2 thin films, (2019).

[21] A.K. Singh, U.T. Nakate, Properties of Nanocrystalline Zirconia, The Scientific World Journal. 2014 (2014) 349457. https://doi.org/10.1155/2014/349457

[22] S. Gowri, R. Rajiv Gandhi, M. Sundrarajan, Structural, optical, antibacterial and antifungal properties of zirconia nanoparticles by biobased protocol, Journal of Materials Science and Technology. 30 (2014) 782-790. https://doi.org/10.1016/j.jmst.2014.03.002

[23] S.N. Basahel, T.T. Ali, M. Mokhtar, K. Narasimharao, Influence of crystal structure of nano-sized ZrO2 on photocatalytic degradation of methyl orange, Nanoscale Research Letters. 10 (2015). https://doi.org/10.1186/s11671-015-0780-z

[24] S. Biswas, M. Bal, S.K. Behera, T.K. Sen, B.C. Meikap, Process optimization study of Zn 2+ + adsorption on biochar-alginate composite adsorbent by response surface methodology (RSM), Water (Switzerland). 11 (2019). https://doi.org/10.3390/w11020325

[25] R.R. Karri, M. Tanzifi, M. Tavakkoli Yaraki, J.N. Sahu, Optimization and modeling of methyl orange adsorption onto polyaniline nano-adsorbent through response surface method-

ology and differential evolution embedded neural network, Journal of Environmental Management. 223 (2018) 517-529. https://doi.org/10.1016/j.jenvman.2018.06.027
[26] S.A. Khan, Z. Fu, S.S. Rehman, M. Asif, W. Wang, H. Wang, Study of template-free synthesis hierarchical m-ZrO2 nanorods by hydrothermal method, Powder Technology. 256 (2014) 71-74. https://doi.org/10.1016/j.powtec.2014.02.012
[27] K.M. Reza, A. Kurny, F. Gulshan, Parameters affecting the photocatalytic degradation of dyes using TiO2: a review, Applied Water Science. 7 (2017) 1569-1578. https://doi.org/10.1007/s13201-015-0367-y
[28] S. Archana, D. Radhika, B.K. Jayanna, K. Kannan, K. Yogesh Kumar, H.B. Muralidhara, Functionalization and partial grafting of the reduced graphene oxide with p-phenylenediamine: An adsorption and photodegradation studies, Elsevier B.V., 2020. https://doi.org/10.1016/j.flatc.2020.100210
[29] M. Kumaresan, K. Vijai Anand, K. Govindaraju, S. Tamilselvan, V. Ganesh Kumar, Seaweed Sargassum wightii mediated preparation of zirconia (ZrO 2) nanoparticles and their antibacterial activity against gram positive and gram negative bacteria, Microbial Pathogenesis. 124 (2018) 311-315. https://doi.org/10.1016/j.micpath.2018.08.060
[30] G. Pradhaban, G.S. Kaliaraj, V. Vishwakarma, Antibacterial effects of silver-zirconia composite coatings using pulsed laser deposition onto 316L SS for bio implants, Progress in Biomaterials. 3 (2014) 123-130. https://doi.org/10.1007/s40204-014-0028-5
[31] N. Tabassum, D. Kumar, D. Verma, R.A. Bohara, M.P. Singh, Zirconium oxide (ZrO2) nanoparticles from antibacterial activity to cytotoxicity: A next-generation of multifunctional nanoparticles, Materials Today Communications. 26 (2021) 102156. https://doi.org/10.1016/j.mtcomm.2021.102156
[32] A. Sirelkhatim, S. Mahmud, A. Seeni, N.H.M. Kaus, L.C. Ann, S.K.M. Bakhori, H. Hasan, D. Mohamad, Review on zinc oxide nanoparticles: Antibacterial activity and toxicity mechanism, Nano-Micro Letters. 7 (2015) 219-242. https://doi.org/10.1007/s40820-015-0040-x
[33] M.H. Sayadi, N. Ahmadpour, S. Homaeigohar, Photocatalytic and Antibacterial Properties of Ag-CuFe2O4@WO3 Magnetic Nanocomposite, Nanomaterials 2021, Vol. 11, Page 298. 11 (2021) 298. https://doi.org/10.3390/nano11020298
[34] N. Al-Zaqri, A. Muthuvel, M. Jothibas, A. Alsalme, F.A. Alharthi, V. Mohana, Biosynthesis of zirconium oxide nanoparticles using Wrightia tinctoria leaf extract: Characterization, photocatalytic degradation and antibacterial activities, Inorganic Chemistry Communications. 127 (2021) 108507. https://doi.org/10.1016/j.inoche.2021.108507
[35] S.A. Khan, Z. Fu, S.S. Rehman, M. Asif, W. Wang, H. Wang, Study of template-free synthesis hierarchical m-ZrO2 nanorods by hydrothermal method, Powder Technology. 256 (2014) 71-74. https://doi.org/10.1016/j.powtec.2014.02.012
[36] A. Mai-Prochnow, M. Clauson, J. Hong, A.B. Murphy, Gram positive and Gram negative bacteria differ in their sensitivity to cold plasma, Scientific Reports 2016 6:1. 6 (2016) 1-11. https://doi.org/10.1038/srep38610